JACS
JOURNAL OF THE AMERICAN CHEMICAL SOCIETY
pubs.acs.org/JACS

Article

Proton Transfer Kinetics in Histidine Side Chains Determined by pH-Dependent Multi-Nuclear NMR Relaxation

Heiner N. Raum, Kristofer Modig, Mikael Akke, and Ulrich Weininger*

Cite This: J. Am. Chem. Soc. 2024, 146, 22284−22294

Read Online

ACCESS | Metrics & More | Article Recommendations | Supporting Information

ABSTRACT: Histidine is a key amino-acid residue in proteins with unique properties engendered by its imidazole side chain that can exist in three different states: two different neutral tautomeric forms and a protonated, positively charged one with a pK_a value close to physiological pH. Commonly, two or all three states coexist and interchange rapidly, enabling histidine to act as both donor and acceptor of hydrogen bonds, coordinate metal ions, and engage in acid/base catalysis. Understanding the exchange dynamics among the three states is critical for assessing histidine's mechanistic role in catalysis, where the rate of proton exchange and interconversion among tautomers might be rate limiting for turnover. Here, we determine the exchange kinetics of histidine residues with pK_a values representative of the accessible range from 5 to 9 by measuring pH-dependent ^{15}N, ^{13}C, and ^{1}H transverse relaxation rate constants for 5 nuclei in each imidazole. Proton exchange between the imidazole and the solvent is mediated by hydronium ions at acidic and neutral pH, whereas hydroxide mediated exchange becomes the dominant mechanism at basic pH. Proton transfer is very fast and reaches the diffusion limit for pK_a values near neutral pH. We identify a direct pathway between the two tautomeric forms, likely mediated by a bridging water molecule or, in the case of high pH, hydroxide ion. For histidines with pK_a 7, we determine all rate constants (lifetimes) involving protonation over the entire pH range. Our approach should enable critical insights into enzymatic acid/base catalyzed reactions involving histidines in proteins.

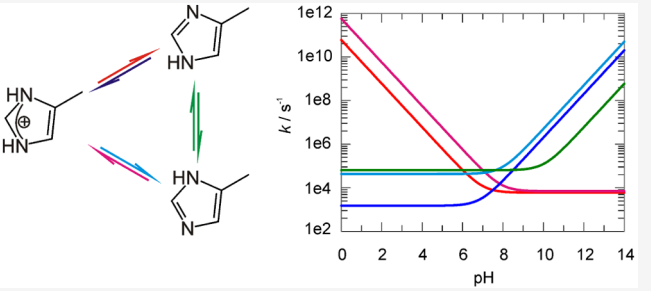

INTRODUCTION

Histidine, a key amino acid in proteins, possesses a unique chemical property—the imidazole moiety of its side chain—that endows it with great versatility in biochemical processes. The two nitrogen atoms of the imidazole ring can undergo protonation and deprotonation, resulting in three possible states: two neutral tautomers in which only one of the nitrogens is protonated (either HNε2 or HNδ1),[1,2] and the doubly protonated and positively charged state (His$^+$); see Figure 1. Because the intrinsic pK_a values are usually close to physiological pH and the free energy difference between the two tautomeric states is relatively small, histidine commonly coexists in two or three states that interconvertrapidly.[3] Thus, the equilibrium between the different states is exquisitely sensitive to factors such as pH, electrostatic interactions, and hydrogen bonding. These features make histidine the chemically most versatile amino acid, and it is often engaged in catalysis.[4,5] In fact, histidine has many different functions: it can act as a nucleophile and as an acid/base catalyst,[6,7] e.g., in catalytic triads,[8,9] as a proton shuttle,[10,11] as a hydrogen bond donor and acceptor,[12,13] and it can coordinate metal ions.[14] Hydrogen bonding involving histidine is of particular interest in the context of protein structure. Histidine can serve as both a hydrogen bond donor and acceptor, making it a pivotal participant in intricate networks of interactions within protein

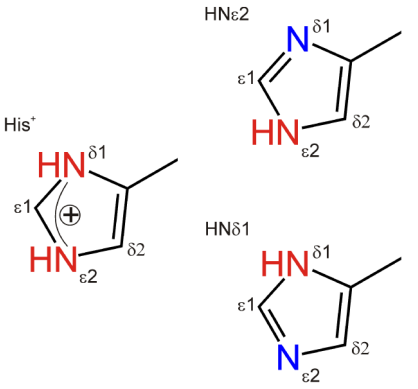

Figure 1. Protonation states of histidine. Protonated (left), neutral HNε2 (upper right), neutral HNδ1 (lower right). Proton and hydrogen bond donors are colored red, proton and hydrogen bond acceptors are blue. Positions within the imidazole ring are labeled.

Received: April 4, 2024
Revised: June 14, 2024
Accepted: July 1, 2024
Published: August 5, 2024

active sites. Hydrogen bonds not only stabilize the protonation state of the imidazole, but also influence its pK_a, thereby regulating its reactivity. The ability of histidine to act as a proton shuttle, facilitating proton transfer reactions between reactants during enzymatic catalysis, underscores its indispensable role in diverse biochemical pathways. Histidine mediated hydrogen bonds can be of crucial functional relevance, as in photosystem II[15,16] or Pin1.[17] Furthermore, histidine plays a key role in regulating ion channels.[18,19] Understanding the protonation kinetics of the histidine side chain is fundamental to unraveling the mechanisms underlying these properties.

Solution NMR spectroscopy has a long history of investigating the configuration of individual histidines at equilibrium. ^{15}N and ^{13}C chemical shifts within the imidazole moiety are clearly indicative of the three different states (His$^+$, HNε2, and HNδ1). The ^{13}Cδ2 chemical shift is diagnostic of the HNδ1 tautomeric state,[20,21] as is the ^{13}Cγ shift of the HNε2 tautomeric state. However, the latter nucleus is less readily monitored, because it does not have a directly attached proton. The ^{13}Cε1 and ^{1}Hε1 chemical shifts are both sensitive to protonation (i.e., formation of the His$^+$ state) and therefore serve as reporters in pH titration experiments to determine the pK_a value.[22−24] The chemical shifts of both imidazole nitrogens (^{15}Nδ1 and ^{15}Nε2) are almost exclusively dependent on the protonation or tautomeric state of the histidine, rather than on their position in the ring[20] or the tertiary structure. The shift of a nonprotonated nitrogen (having a free electron pair) is completely different from that of a protonated nitrogen (250 ppm compared to 170−180 ppm).

NMR spectroscopy is a powerful tool for studying microsecond-to-millisecond exchange processes by relaxation dispersion methods.[25,26] While these methods are often applied to study conformational changes affecting multiple residues,[27,28] distinct local events of side chains like aromatic ring-flips[29−31] or protonation kinetics of aspartates and glutamates[32] can also be investigated. Exchange between the two tautomeric states of histidine has been quantified previously for the special case where it is coupled to conformational exchange, as demonstrated in plastocyanin using a combination of pH titration and backbone relaxation dispersion methods,[33] and also in FKBP12 by aromatic ^{13}C based relaxation dispersion methods.[3] Since the chemical shifts of the imidazole ring are sensitive reporters on the different tautomeric forms, the populations of the tautomeric states can be quantified,[34,35] as has been reported for a high-energy state of Im7.[36] However, the methods applied in that study are limited to relatively slow exchange processes (<100 s^{-1}). Proton exchange rates not coupled to conformational exchange have previously been determined only for the free histidine amino acid[37] with rates up to 85,000 s^{-1}. So far, studies on proton exchange kinetics have been limited to small molecules[7] and to measurements on proteins at a single pH, except for the case of aspartates and glutamates.[32] The kinetic mechanism of histidine tautomerization also has been unresolved.

Here we determine the proton exchange kinetics of histidine side chains by measuring the pH dependence of transverse relaxation rate constants (R_2) for several ^{15}N, ^{13}C, and ^{1}H resonances in each histidine side chain. We studied three histidine residues with pK_a values of 5, 7, and 9, so as to cover a wide range of conditions. Our studies reveal that the dominant mechanism of proton exchange between histidine and the solvent switches from being proton mediated at pH 7 to hydroxide mediated at pH 9. For histidines with a neutral pK_a, the protonation on-rate constant reaches the theoretical diffusion limit with a rate of about 4×10^{11} M^{-1} s^{-1}, which includes both diffusion of the ions and proton jumping[38] between hydronium ions.[32] It should be noted that solvated protons can exist not only as hydronium ions but alternatively as higher-order hydration species (so-called Eigen or Zundel forms);[5] from here on we refer to these as hydronium ions or H_3O^+. We find that protons exchange directly between the two neutral tautomeric forms, mediated by a bridging water molecule at low and neutral pH, or by hydroxide at high pH. Furthermore, we establish a connection between thermodynamic and kinetic parameters (pK_a values and k_{on} or k_{off} rate constants) for the H_3O^+/H_2O mediated proton exchange mechanism, in the case of maximal (structurally unhindered) proton exchange. For the histidine with a pK_a value of 7, typical for functionally relevant histidines, our analysis yields rate constants and lifetimes over the entire pH range. Our approach provides a framework to investigate the biophysical basis for enzymatic acid/base catalyzed reactions involving histidines.

RESULTS AND DISCUSSION

In this article we investigate proton exchange in three histidines, H22 and H51 in the *rhh* protein of plasmid pRN1 from *Sulfolobus islandicus*,[39] and H31 in T4 lysozyme. These three histidines have been chosen because they exhibit different pK_a values (around 5, 7, and 9, respectively) and qualitatively different tautomer equilibria, namely equal populations of HNδ1 and HNε2 (H22), dominated by HNε2 (H51), and dominated by HNδ1 (H31). Each of these histidines populates a single side-chain rotamer in the crystal structure, is fairly solvent exposed, does not have any ionizable groups with similar pK_a values nearby, and does not exhibit any negative cooperativity in their pH titration behavior. H31 Nδ1 is a hydrogen-bond donor to D70 (pK_a 0.5), which stabilizes the positively charged state of H31 and its HNδ1 tautomer. H51 shows no particular structural features, thus displaying a rather generic behavior in terms of pK_a and tautomer. H22 shows no particular favorable interaction, but disfavors the positively charged state. In the following, we present a set of parsimonious models of increasing complexity, capable of describing the proton exchange, and then proceed to analyze the experimental pH-dependent R_2 data using these models. For brevity, we focus in the main text on the model that best explains the exchange behavior of a given histidine, while the Supporting Information includes the fits of the other models to the experimental data. We compare kinetic data (k_{on} and k_{off}) with thermodynamic data (pK_a values) and establish general rules for their relationship, including the effects of diffusion limited exchange. We finish by calculating protonation rate constants and lifetimes for the different states of histidine in a pH dependent manner.

Kinetic models of varying complexity can be used to describe the chemical equilibria relating to the three different states of histidine side chains defined as the protonated, positively charged state (His$^+$) and the two neutral tautomers (HNε2 and HNδ1). We define the rate constants of the different reactions as follows: k_{on} is the rate constant of the reaction going from a neutral state to His$^+$, in which a proton is binding to the imidazole; k_{off} is the rate constant of the reaction from His$^+$ to a neutral state, in which a proton is

https://doi.org/10.1021/jacs.4c04647
J. Am. Chem. Soc. 2024, 146, 22284−22294

leaving the imidazole; and k_{taut} is the rate constant of the reaction interconverting the two neutral tautomers.

Two-State Exchange Model. The simplest kinetic model is a pseudo two-state model (model I, Figure 2A), consisting of the protonated positively charged state (His^+) and the neutral state, without discriminating between the two tautomers (HNε2 + HNδ1). Under certain conditions it is permissible to use this model because the chemical shifts of some nuclei, especially ^{1}Hε1 and ^{13}Cε1, in the histidine side chain are very sensitive to the population of the protonated state, but rather independent of the relative populations of the two neutral tautomers. This model closely resembles a previous approach used to extract protonation and deprotonation rate constants for Asp and Glu side chains,[32] which can exist only in two states: a protonated, neutral state or a deprotonated, negatively charged one. The pseudo two-state model can be subdivided into H_3O^+/H_2O mediated proton exchange (model Ia, Figure S1A), with H_3O^+ as the pH dependent proton donor and H_2O as the pH independent proton acceptor, as was observed in the Asp and Glu study for pK_a values between 2 and 6.5,[32] and H_2O/OH^- mediated proton exchange (model Ib, Figure S1B), with H_2O as the pH independent proton donor and OH^- as the pH dependent proton acceptor, for higher pK_a values. These two models can be distinguished by the difference in the position of the maximal exchange contribution (R_{ex}) plotted as a function of pH (Figure 2B). In the case of H_3O^+/H_2O mediated proton exchange, the maximum is positioned at 0.3 pH units higher than the pK_a value, whereas for H_2O/OH^- mediated proton exchange it is positioned at 0.3 units lower than pK_a.[32]

Linear Three-State Exchange Model. The chemical shifts of ^{13}Cδ2, ^{15}Nδ1, and ^{15}Nε2 carry information about the two neutral tautomers. For each of these nuclei the chemical shifts in the HNδ1 tautomer is distinct from shifts in the HNε2 tautomer and the protonated form, which can be mutually similar. Therefore, by including these nuclei it is possible to use more complex three-state models that provide insight into histidine tautomerization. Thus, if the HNε2 tautomer dominates the neutral form, the minor population of HNδ1 can be determined with high accuracy. On the other hand, if the HNδ1 tautomer dominates the neutral form, it is hard to distinguish HNε2 from the protonated state, and the ratio of the two neutral tautomers will be less well determined. The simplest kinetic model of higher complexity is a linear three-state model (model II), which includes exchange between the positively charged state (His^+) and the two neutral states (HNε2 or HNδ1), but neglects exchange between the two neutral states. Again, the proton exchange can be either H_3O^+/H_2O mediated (model IIa, Figure S1C) or H_2O/OH^- mediated (model IIb, Figure S1D).

Triangular Three-State Exchange Model. The most complex kinetic model is a triangular three-state model (model III) that allows for direct exchange between the neutral tautomers (Figure 3A). As pointed out for the linear three-state model, the proton exchange between the protonated state and the neutral states can be mediated by H_3O^+/H_2O or H_2O/OH^- (model IIIa or IIIb Figure S1EG/FH). For exchange between the two neutral tautomers, H_3O^+ catalyzed exchange can be excluded, because this would involve an intermediate step via the protonated state (His^+). This leaves as the only possibilities OH^- catalyzed exchange (model IIIa/b + c, Figure S1E and F), water catalyzed exchange (model IIIa/b + d, Figure S1G and H) or a combination of both (model IIIa/b + cd, Figure S1E−H).

Overview of pH-Dependent R_2 Relaxation Rate Constants. We determined the pH dependence of R_2 relaxation rate constants for three histidine residues: H22 and H51 of the *rhh* protein[39] and H31 of T4 lysozyme, which titrate in three different regimes with pK_a values of 4.89, 6.94 and 8.95, respectively (Figure 2C,D).

Below, we first describe the exchange between the protonated form (His^+) and the two neutral forms (HNε2 and HNδ1) using the pseudo two-state model by analyzing R_2 vs pH profiles measured for ^{1}Hε1 and ^{13}Cε1. These profiles display close similarities to those obtained in a previous study on proton exchange in aspartates and glutamates, observed by ^{13}C relaxation.[32] We determine the exchange mechanisms (H_3O^+/H_2O or H_2O/OH^- mediated) active in the different pH regimes by taking advantage of the different pK_a values of the three residues. Second, we analyze the full relaxation data set (including also ^{13}Cδ2, ^{15}Nδ1, and ^{15}Nε2) using the three-state models describing proton exchange between the three states of each histidine.

Protonation−Deprotonation Exchange in Histidines is Mediated by Hydronium Ions at pH 7 or Below and by Hydroxide Ions at pH 9 or Above. The pH dependence of R_2 relaxation rate constants for the ^{1}Hε1 and ^{13}Cε1 spins reveal exchange between His^+ and the neutral forms, because the chemical shifts of these nuclei are highly sensitive to protonation of the imidazole. For all three residues we observe a prominent R_{ex}-driven increase in R_2 for ^{1}Hε1 (Figure 2C) around the pK_a value in question, but much less so for ^{13}Cε1 (Figure 2D). This result is explained by the greater chemical shift difference ($\Delta\omega$) between the exchanging states for ^{1}Hε. Fast processes (high k_{ex}) lead to an increase in R_{ex} only if $\Delta\omega$ is sufficiently large. The absence of a pronounced increase in R_2 for ^{13}Cε1, however, does serve to establish a lower limit of k_{ex}, since slower processes (low k_{ex}) would lead to an increase in R_{ex} also for smaller $\Delta\omega$. The most pronounced increase in R_2 can be observed for H51 around its pK_a value of 6.9, directly pointing to a slower proton exchange rate around pH 7. Furthermore, the maximum of the R_2 vs pH profile of H51 shows the expected shift by 0.3 pH units toward higher pH values[32] (Figure 2B,C). This shift provides direct evidence of a H_3O^+/H_2O mediated proton exchange mechanism at pH 7 and below, in agreement with findings for Glu and Asp, for which this mechanism was established at pH values up to 6.5.[32]

Analyzing the R_2 vs pH profiles for ^{1}Hε1 and ^{13}Cε1 using the H_3O^+/H_2O mediated proton exchange model (model Ia) results in a reasonable to excellent description of the experimental data for H22 and H51 with k_{ex} rate constants of 15×10^5 s^{-1} and 0.8×10^5 s^{-1} at their pK_a values of 4.86 ± 0.03 and 6.88 ± 0.01, respectively. From these values, we calculate the proton off- and on-rate constants at pH = pK_a, yielding $k_{off}^{(H_2O)} = k_{ex}/2 = (7.5 \pm 0.7) \times 10^5$ s^{-1} for H22 and $(0.41 \pm 0.04) \times 10^5$ s^{-1}for H51, and $k_{on}^{(H_3O+)} = k_{ex}/(2\,[H^+]) = (0.54 \pm 0.06) \times 10^{11}$ M^{-1} s^{-1} and $(3.1 \pm 0.3) \times 10^{11}$ M^{-1} s^{-1}, respectively. Notably, $k_{on}^{(H_3O+)}$ for H51 is in the range expected for a diffusion limited reaction, while for H22 it is 1 order of magnitude below the diffusion limit. Not exceeding the diffusion limit serves as an additional quality control of the results.

In contrast to the case of H22 and H51,model Ia does not describe the experimental data for H31 in a satisfactory way

https://doi.org/10.1021/jacs.4c04647
J. Am. Chem. Soc. 2024, 146, 22284−22294

(Figure S2). Using instead the H_2O/OH^- mediated proton exchange model (model Ib) to analyze H31, we obtain an excellent description of the experimental data with an exchange rate constant of 1.4×10^5 s^{-1} at the pK_a value of 9.00 ± 0.02, which translated into proton off- and on-rate constants of $k_{on}^{(H_2O)}$= (0.72 ± 0.06) × 10^5 s^{-1} and $k_{off}^{(OH-)}$= (0.7 ± 0.1) × 10^{10} M^{-1} s^{-1}. Here, $k_{on}^{(H_2O)}$denotes proton exchange from water to histidine (pH independent, hence in units of s^{-1}), and $k_{off}^{(OH-)}$denotes exchange from histidine to hydroxide (pH dependent, hence in units of M^{-1} s^{-1}). $k_{off}^{(OH-)}$ is almost an order of magnitude below the diffusion limit observed for $k_{on}^{(H_3O+)}$ of H51. The results obtained using the pseudo two-state model are summarized in Table 1. Combining the findings for all three histidines we observe a switch in the dominant proton exchange mechanism from H_3O^+/H_2O mediated at pH ≤ 7 to H_2O/OH^- mediated at pH ≥ 9.

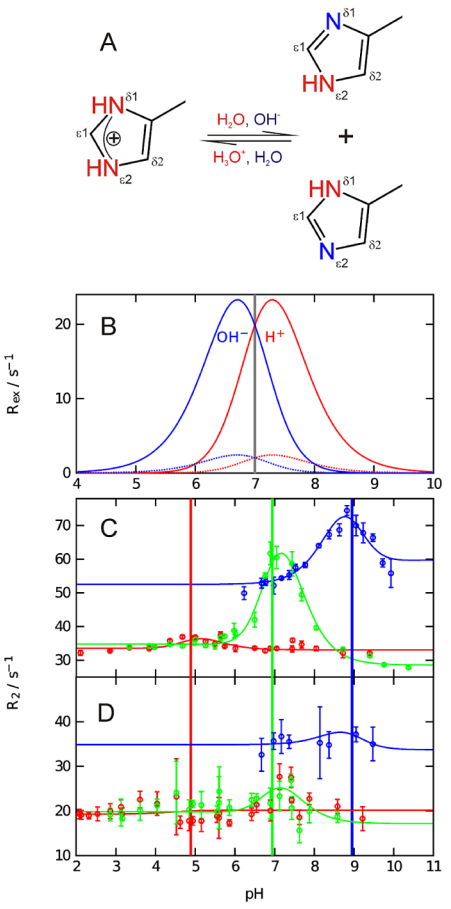

Figure 2. Pseudo two-state proton exchange in histidine (A). The H_3O^+/H_2O mediated exchange mechanism is colored red, and the H_2O/OH^- mediated exchange mechanism is colored blue. Theoretical R_2 vs pH profiles for H_3O^+/H_2O (red) and H_2O/OH^- (blue) mediated exchange for pK_a 7.0 (vertical gray line).(B) Profiles for faster exchange processes are shown as dashed lines, for slower exchange processes as solid lines. Experimental $^1H\varepsilon1$ (C) and $^{13}C\varepsilon1$ (D) R_2vs pH profiles for *rhh* proteinH22 (red), *rhh* protein H51 (green), and T4-Lysozyme H31 (blue). pK_a values are shown as vertical lines. Solid lines represent pseudo two-state fits (eqs 11 and 12) using the H^+ (H22 and H51) (eq 5) or OH^- (H31) (eq 6) catalyzed models. Results of the pseudo two-state fits are summarized in Table 1.

Table 1. pK_a Values and Rate Constants From the Pseudo Two-State Exchange Model

residue	H22	H51	H31
pK_a	4.86 ± 0.03	6.88 ± 0.01	9.00 ± 0.02
$k_{on}^{(H_3O+)}$(×10^{11} M^{-1} s^{-1})	0.54 ± 0.06	3.1 ± 0.3	
$k_{off}^{(H_2O)}$(× $10^5 s^{-1}$)	7.5 ± 0.7	0.41 ± 0.04	
$k_{on}^{(H_2O)}$(× 10^5 s^{-1})			0.72 ± 0.06
$k_{off}^{(OH-)}$(×10^{11} M^{-1} s^{-1})			0.07 ± 0.01

The H_3O^+/H_2O mediated $k_{on}^{(H_3O+)}$ at pH 7 (3.4×10^{11} M^{-1} s^{-1}) is about 50 times higher than the H_2O/OH^- mediated $k_{off}^{(OH-)}$ at pH 9 (0.07×10^{11} M^{-1} s^{-1}), showing that the H_3O^+/H_2O mediated proton exchange mechanism is more efficient. However, between pH 7 and 9 the proton to hydroxide ratio changes by a factor of 10,000—more than enough to induce a change in mechanism. Considering the derived rate constants and the relevant proton (hydronium) and hydroxide concentrations, we find that the two mechanisms are equally efficient (have equal proton exchange rates) at pH 7.8.

A Triangular Exchange Model Explains the R_2 vs pH Profiles for All Histidine Nuclei. In order to describe in more detail, the exchange between the two neutral tautomeric forms and the protonated form of histidine, we analyzed the pH dependence of the R_2 values of $^{13}C\delta2$, $^{15}N\delta1$. and $^{15}N\varepsilon2$ (Figure 3). The chemical shifts of these nuclei are sensitive reporters on the two neutral tautomeric states. Based on H51, for which the most complete and distinct R_2 profiles could be determined for all five positions ($^1H\varepsilon1$, $^{13}C\varepsilon1$, $^{13}C\delta2$, $^{15}N\delta1$, and $^{15}N\varepsilon2$) over a large pH range, we analyzed the different three-state models. We rejected the linear three-state model (model IIa, Figure S3). An expanded the model to a water catalyzed proton transfer pathway that directly connects the two tautomers (model IIIa + d) only describes the data up to pH 9 (Figure S4 left). The triangular exchange model (Figure 3A) with an additional hydroxide-dependent pathway between the two neutral tautomers (model IIIa + cd), describes all data for H51 (Figure S5 right) and therefore is the correct model to describe proton exchange in histidine, if sufficient data is available, as for H51 (Figure 3). Note that the direct pathway between tautomers likely involves a bridging water molecule or hydroxide ion that shuttles the proton between sites. In the case of H22, the nuclei sensitive to tautomerization ($^{13}C\delta2$, $^{15}N\delta1$, and $^{15}N\varepsilon2$) could only be monitored for pH values between 2 and 6, due to severe exchange broadening resulting from equal population of the two tautomers. Due to the lack of data at higher pH the hydroxide-mediated exchange between tautomers cannot be included in the model for H22, which instead includes only H_3O^+/H_2O mediated proton exchange between the His^+ state and the two tautomeric states in combination with water catalyzed tautomer exchange (model IIIa + d), with certain restrictions (see Experimental section). All this leads to a somewhat reduced quality of the fit (Figure 3D red), but the overall features are captured. In the case of H31 we included H_2O/OH^- mediated proton exchange between the His^+ state and the two tautomeric states, but did not include exchange between the two tautomeric forms (model IIb), because H31 exists predominantly in the HN$\delta1$ tautomer at high pH, and therefore R_2 values for $^{13}C\delta2$ have only a very minor contribution from exchange due to tautomerization.

https://doi.org/10.1021/jacs.4c04647
J. Am. Chem. Soc. 2024, 146, 22284−22294

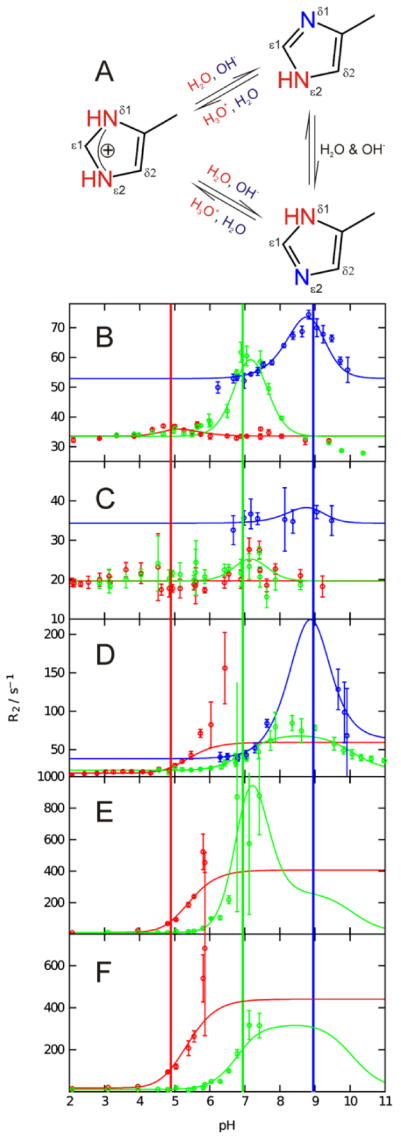

Figure 3. Triangular three-state proton exchange in histidine. (A) The H_3O^+/H_2O mediated exchange mechanism is colored red, the H_2O/OH^- mediated exchange mechanism is colored blue. The H_2O and OH^- catalyzed tautomerization is colored black. Experimental $^1H\varepsilon1$ (B), $^{13}C\varepsilon1$ (C), $^{13}C\delta2$ (D), $^{15}N\delta1$ (E), and $^{15}N\varepsilon2$ (F) R_2 vs pH profiles for *rhh* protein H22 (red), *rhh* proteinH51 (green) and T4-Lysozyme H31 (blue). pK_a values are shown as vertical lines. Solid lines represent triangular three-state fits (eqs 13 and 14), combined with eqs 3, 4, 7, 9 and 5 (H22), eq 6 (H31) or both (H51). In case of $^{15}N\delta1$ (E) and $^{15}N\varepsilon2$ (F) values for the neutral tautomers at high pH cannot be obtained, because of their small $^{13}C-^{15}N$ J-coupling, in addition to severe exchange broadening. Results of the triangular three-state fits are summarized in Table 2.

The final results are summarized in Table 2. Briefly, H22 displays microscopic pK_a values of 5.18 ± 0.02 and 5.09 ± 0.02 for Nε2 and Nδ1, respectively, $k_{on}^{(H_3O+)}$of (0.67 ± 0.04) × 10^{11} M^{-1} s^{-1} and (0.67 ± 0.04) × 10^{11} M^{-1} s^{-1}, $k_{off}^{(H_2O)}$of (4.4 ± 0.4) × 10^5 s^{-1} and (5.4 ± 0.4) × 10^5 s^{-1}, and $k_{taut\uparrow}^{(H_2O)}$of (1.6 ± 0.1) × 10^5 s^{-1}. The individual pK_a values are higher than the overall pK_a value of the 2-state approach (4.86 ± 0.03), see Figure 4, red symbols. This difference in pK_a values reflects the difference between the two models, as follows. The overall pK_a value derived by the 2-state approach represents the pH where the relative population of the doubly protonated His^+ state and the singly protonated, uncharged state both are 50%, where the latter comprises both tautomers, so that in total 75% of the nitrogens are protonated. In contrast, the 3-state approach yields the individual pK_a values for the nitrogens so that 50% of the site is protonated at pH = pK_a. Therefore, the individual pK_a values are always equal to higher than the overall (two-state) pK_a value, since reaching the protonation level corresponding to the overall (two-state) pK_a value, since reaching the protonation level corresponding to the overall pK_a value requires that both individual sites be protonated by more than 50%. In terms of the rate constants, there is good agreement (Figure 4) with the values of $k_{on}^{(H_3O+)}$ and $k_{off}^{(H_2O)}$ determined from the two-state approach, (0.54 ± 0.05) × 10^{11} M^{-1} s^{-1} and (7.5 ± 0.7) × 10^5 s^{-1}. Therefore, the results from the two-state approach provide good estimates of the individual protonation kinetics, unless the proton exchange on one of the nitrogens is heavily slowed down by structural restrictions. In that case, the results from the two-state approach would only provide good estimates of the proton exchange on the faster exchanging nitrogen.

Also, in the case of H51 the pK_a values of Nε2 (7.60 ± 0.05) and Nδ1 (7.12 ± 0.02) are higher than the pK_a value for the two-state approach (6.88 ± 0.02), for the reasons described above. For H51 both the H_3O^+/H_2O and H_2O/OH^- mediated proton exchange mechanisms were included in the triangular three-state model. The $k_{on}^{(H_3O+)}$ values determined for Nε2 and Nδ1 are (0.6 ± 0.1) × 10^{11} M^{-1} s^{-1} and (5.7 ± 0.3) × 10^{11} M^{-1} s^{-1}, respectively, and the $k_{off}^{(H_2O)}$values are (0.015 ± 0.004) × 10^5 s^{-1} and (0.43 ± 0.03) × 10^5 s^{-1}, in case of H_3O^+/H_2O mediated proton exchange. There is a good agreement (Figure 4) between these values derived for Nδ1 and those determined by the two-state approach, (3.1 ± 0.3) × 10^{11} M^{-1} s^{-1} and (0.41 ± 0.04) × 10^5 s^{-1}, because proton exchange at the Nδ1 position is fast and unrestricted by structural features. In contrast, the two-state model cannot capture the slower exchange observed for Nε2. Nevertheless, the overall proton exchange affecting H51 is well described by the two-state model. Values determined for the H_2O/OH^- mediated proton exchange mechanism are about a factor of 10 lower, with $k_{off}^{(OH-)}$of (0.2 ± 0.1) and (0.5 ± 0.1) × 10^{11} M^{-1} s^{-1} and $k_{on}^{(H_2O)}$ values are (0.06 ± 0.05) and (0.07 ± 0.02) × 10^5 s^{-1}, demonstrating again that H_3O^+/H_2O mediated proton exchange is more efficient and thus the dominating exchange mechanism slightly above pH 7. Values for the direct proton transfer between the two tautomers are $k_{taut\uparrow}^{(H_2O)}$of (0.64 ± 0.06) × 10^5 s^{-1} for the water catalyzed exchange mechanism and $k_{taut\uparrow}^{(OH-)}$of (5.9 ± 0.2) × 10^8 M^{-1} s^{-1} for OH^- catalyzed exchange.

We analyzed H31 using the H_2O/OH^- mediated proton exchange model. The results for Nε2 and Nδ1 yield pK_a values of 9.10 ± 0.01 and 10.0 ± 0.1, which again are higher than the value fitted using the two-state model, pK_a = 9.00 ± 0.02. Since H31 exists almost exclusively in the neutral HNδ1 tautomer, the pK_a value at Nδ1 is significantly higher, resulting in almost complete protonation of Nδ1 already at pH values where Nε2 first starts to become protonated. The protonation midpoint of Nδ1 is far from the two-state pK_a value (and from the pK_a value determined by chemical shift titrations), therefore the

https://doi.org/10.1021/jacs.4c04647
J. Am. Chem. Soc. 2024, 146, 22284−22294

Table 2. pK_a Values and Rate Constants From the Triangular Three-State Exchange Model

residue	H22		H51		H31	
position	Nε2	Nδ1	Nε2	Nδ1	Nε2	Nδ1
pK_a	5.18 ± 0.02	5.09 ± 0.02	7.60 ± 0.05	7.12 ± 0.02	9.10 ± 0.01	10.0 ± 0.1
$k_{on}^{(H_3O+)}$(×10^{11} M^{-1} s^{-1})	0.67 ± 0.04	0.67 ± 0.04	0.6 ± 0.1	5.7 ± 0.3		
$k_{on}^{(H_2O)}$(× $10^5 s^{-1}$)	4.4 ± 0.4	5.4 ± 0.4	0.015 ± 0.004	0.43 ± 0.03		
$k_{on}^{(H_2O)}$(× $10^5 s^{-1}$)			0.06 ± 0.05	0.07 ± 0.02	0.55 ± 0.03	56 ± 7000
$k_{off}^{(OH-)}$(×10^{11} M^{-1} s^{-1})			0.2 ± 0.1	0.5 ± 0.1	0.044 ± 0.002	0.6 ± 5
$k_{taut\uparrow}^{(H_2O)}$(× $10^5 s^{-1}$)	1.6 ± 0.1		0.64 ± 0.06			
$k_{taut\uparrow}^{(OH-)}$(× 10^8 M^{-1} s^{-1})			5.9 ± 0.2			

results for Nδ1 have poor precision and are unreliable (see Table 2 for the fitted values and estimated errors). The analysis of the Nε2 data results in $k_{off}^{(OH-)}$= (0.044 ± 0.002) × 10^{11} M^{-1} $s^{-1}$and $k_{on}^{(H_2O)}$= (0.55 ± 0.03) × 10^5 s^{-1}. These results are close to the ones from the 2-state model, $k_{off}^{(OH-)}$ = (0.07 ± 0.01) × 10^{11} M^{-1} s^{-1} and $k_{on}^{(H_2O)}$= (0.72 ± 0.06) × 10^5 s^{-1}. However, the steep rise in the ^{13}Cδ2 profile compared to the^{1}Hε1 profile cannot be explained without including a minor population of the HNε2 tautomer.

Comparison of Exchange Rate Constants and pK_a Values: General Aspects and Linear Free-Energy Relationships. To investigate the potential for a unified interpretation of the derived exchange rate constants, we plot all rate constants of the three His residues against the corresponding pK_a values (Figure 4). The data include the k_{on} and k_{off} rate constants for both the H_3O^+/H_2O and H_2O/OH^- mediated proton exchange mechanism, determined by both the two-state and triangular three-state approaches. We also include proton k_{on} and k_{off} rate constants for Asp and Glu[32] in order to compare proton exchange in these different side chains and identify possible similarities and general rules. The observed relationship between rate constants and pK_a values can be explained by ideal behavior involving kinetic (k_{on} and k_{off}) and thermodynamic (pK_a) parameters, for example, a 1 unit lower (higher) pK_a value arises from a 10 times lower (higher) k_{on} or 10 times higher (lower) k_{off}. This interpretation holds for theH_3O^+/H_2O mediated proton exchange mechanism for all data except for His51 Nε2. Data points with pK_a < 5.5 follow a linear trend, which can be explained purely by changes in $k_{on}^{(H_3O+)}$ (Figure 4A). At pK_a ≈ 5.5 and above, $k_{on}^{(H_3O+)}$ reaches the diffusion limit, which can be estimated to roughly 4 × 10^{11} M^{-1} s^{-1}. In other words the attachment of protons to ionizable groups below pK_a values of 5.5 is not limited by diffusion, but by other factors stabilizing the nonprotonated state. This is in contrast to the case of ionizable with pK_a values above 5.5, where protonation is indeed diffusion limited. Thus, the data observed for pK_a > 5.5 cannot be rationalized by changes in $k_{on}^{(H_3O+)}$, but are instead caused by changes in $k_{off}^{(H_2O)}$ up until the point where the H_2O/OH^-exchange mechanism becomes dominant (i.e., somewhere between pH 7.5 and 8; Figure 4B) and whereas the H_3O^+/H_2O mediated proton exchange becomes ineffective and thus hard to study. We note that His, Asp and Glu residues all display the same overall trend. Structural aspects appear to not impact the kinetics beyond their effect on the pK_a values. Therefore, for each of these residue types one can directly estimate k_{on} and k_{off} rate constants with sufficient accuracy directly from their known pK_a values provided that proton exchange is unhindered. In contrast, if a residue is hidden in the interior of a protein or otherwise solvent inaccessible, or, in the case of His, if the exchanging proton is stabilized by hydrogen bonds, this would result in lower values of both k_{on} and k_{off}. However, the upper limits of the rate constants, at given pK_a values, are well established by the experimental results. By the same logic one should expect similar relationships, e.g., an one unit higher (lower) pK_a value will arise from a 10 times lower (higher) $k_{off}^{(OH-)}$, or 10 times higher (lower) $k_{on}^{(H_2O)}$, in the case of H_2O/OH^- mediated proton exchange, but there are too few experimental data points to firmly establish the expected trend. The proton exchange between imidazole and the solvent can be determined sufficiently well using the pseudo two-state model (Figure 4, triangles and circles), which requires pH-dependent R_2 data for only ^{1}Hε and ^{13}Cε.

Explicit Protonation Rates and Lifetimes the Three States of Histidines at Different pH Values. So far, we have looked at the relationship between pK_a values and k_{on} and k_{off} rate constants in units of M^{-1} $s^{-1}$and s^{-1}, respectively, in the case of H_3O^+/H_2O mediated proton exchange, and in units of s^{-1} and M^{-1} s^{-1}, respectively, in the case of H_2O/OH^- mediated proton exchange. At any given pH we can calculate the actual proton on and off rate constants (in s^{-1}), and compare them directly to other rate constants, such as catalytic rate constants. For the three histidines in this study, H22, H51, and H31, we calculated the rate constant as a function of pH (Figure 5A). For H51 we have information about both H_3O^+/H_2O and H_2O/OH^- mediated proton exchange, so k_{on} and k_{off} can be plotted for both mechanisms across the entire pH range. For H22 and H31, only theH_3O^+/H_2O or H_2O/OH^- mediated proton exchange pathways could be studied, but not both. Therefore, we limit the analysis to pH regions in which either the H_3O^+/H_2O or H_2O/OH^- mediated proton exchange is the clearly dominant mechanism. For H51 k_{on} increases as pH decreases from 7 to 0, whereas k_{on} is constant between pH 8 and 14 (Figure 5, green solid line). The opposite is observed for k_{off}, which increases with increasing pH between pH 8 and 14, but is constant between pH 0 and 7 (Figure 5, green dashed line). Between pH 7 and 8 a gradual switch between the H_3O^+/H_2O and H_2O/OH^- mediated proton exchange mechanism is observed. From the H51 data one can thus directly estimate the upper limit of proton k_{on} and k_{off} at any pH for histidines with neutral pK_a, and compare these values to functional parameters, such as catalytic rate constants. H22 (pK_a around 5) and H31 (pK_a around 9)

https://doi.org/10.1021/jacs.4c04647
J. Am. Chem. Soc. 2024, 146, 22284−22294

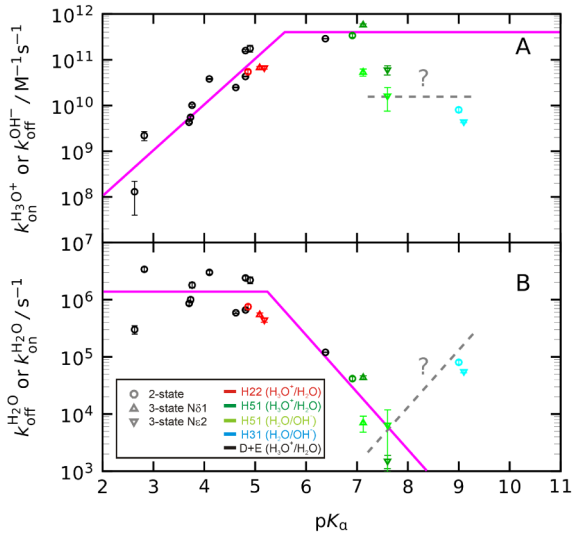

Figure 4. Proton exchange rate constants plotted vs pK_a. Rate constants are plotted on a logarithmic scale, so that the graphs constitute free-energy relationships. Circles and triangles indicate data determined by two-state and three-state models, respectively. Upward and downward pointing triangles represent the imidazole Nδ1 and Nε2 positions, respectively. Color coding of symbols: red, H22 fitted with H_3O^+/H_2O mediated proton exchange mechanism; dark green, H51 fitted with H_3O^+/H_2O mediated proton exchange mechanism; light green, H51 fitted with H_2O/OH^- mediated exchange mechanism; cyan, H31 fitted with H_2O/OH^-mediated proton exchange mechanism. (A) First order H^+ on-rate constants ($k_{on}^{(H_3O+)}$, H_3O^+/H_2O exchange mechanism) and H^+ off-rate constants ($k_{off}^{(OH-)}$, H_2O/OH^-exchange mechanism), both in units of M^{-1} s^{-1} (where the M unit refers to the concentration of H_3O^+ or HO^-). (B) Zero order H^+ off-rate constants ($k_{off}^{(H_2O)}$, H_3O^+/H_2O exchange mechanism) and H^+ on-rate constants ($k_{on}^{(H_2O)}$, H_2O/OH^-exchange mechanism) in units of s^{-1}. Magenta lines represent fits to values (excluding H51 Nε2) derived from the H_3O^+/H_2O exchange mechanism, using ideal slopes (10^{pH}, 0, -10^{pH}) in which only the H^+ on-rate or H^+ off-rate changes with pK_a. Gray dashed lines represent fits with ideal slopes (10^{pH}, 0) to values from the H_2O/OH^- exchange mechanism. Due to the limited data, these lines are speculative and thus indexed with a question mark. It is also unclear if the gray line in panel A should have zero or negative slope; however, because the positive slope of the dashed gray line in panel B is more pronounced by the data, there has to be zero slope in panel A. Black symbols show previously published data for Glu and Asp for comparison.[32] They show the same range and trend as His with similar pK_a values. Histidine data were measured at 23 °C, and Glu−Asp data at 25 °C.

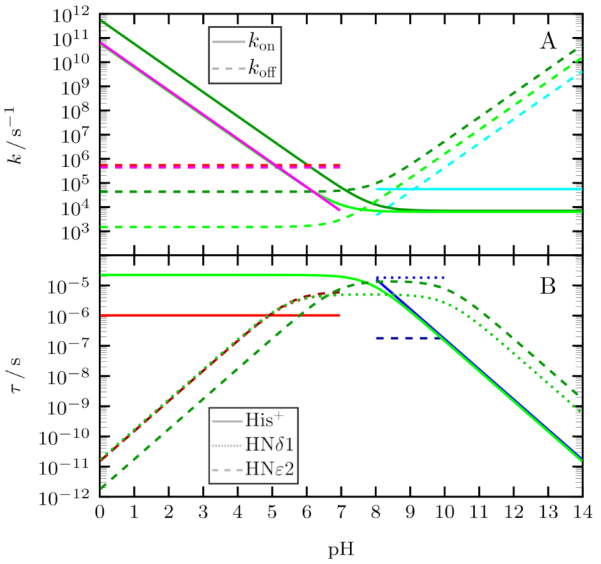

Figure 5. Proton exchange rate constants and life times plotted vs pH. (A) Solid lines represent protonation of the imidazole, dashed lines represent deprotonation, based on experimentally found values and eqs 5, 6, and 10. Colors represent different imidazole sites: H22 Nε2 (magenta), H22 Nδ1 (red), H51 Nε2 (light green), H51 Nδ1 (dark green), and H31 Nε2 (cyan). (B) Solid lines represent the life times of His^+, dashed lines HNε2 and dotted lines HNδ1. The life times of H22 are shown in red tones, of H51 in green tones and of H31 in blue tones. The pH dependence is fully determined for H51, whereas for H22 only proton mediated exchange is characterized and for H31 only hydroxide mediated exchange.

qualitatively confirm the trend observed for H51 in the acidic and basic pH ranges, respectively. In the acidic region, k_{on} is lower and k_{off} is higher for H22 than they are for H51. In the basic region the opposite is observed for H31, i.e., k_{on} is higher and k_{off} is lower for H31 than for H51.

In addition, one can calculate lifetimes for the three states (His^+, HNδ1 and HNε2) of a histidine from the sum of the rate of reactions leading out of the state. Again, for H51 this can be done accurately over the whole pH range since $k_{on}^{(H_3O+)}$, $k_{off}^{(H_2O)}$, $k_{on}^{(H_2O)}$, $k_{off}^{(OH-)}$, $k_{taut\uparrow}^{(H_2O)}$, and $k_{taut\uparrow}^{(OH-)}$ have all been determined. His^+ shows the longest lifetime of around 22 μs below pH 7.5, while its lifetime decreases above pH 7.5. The neutral tautomers HNδ1 and HNε2 have the longest lifetimes of approximately10 μs in the region pH 7−10, but decreasing lifetimes at lower or higher pH. H22 ($k_{on}^{(H_3O+)}$, $k_{off}^{(H_2O)}$, $k_{taut\uparrow}^{(H_2O)}$) and H31 ($k_{on}^{(H_2O)}$, $k_{off}^{(OH-)}$) qualitatively confirm the trend observed for H51 in the acidic and basic pH ranges, respectively. H22 shows a shorter lifetime of 1 μs for His^+, and similar pH dependent lifetimes of HNδ1 and HNε2, all up to pH 7, for which the determination is accurate. H31 shows the same pH dependent lifetime for His^+ as does H51 above pH 8. The lifetimes for HNδ1 (18 μs) and HNε2 (0.2 μs) could only be determined for the pH range 8−10. They fall into the range of lifetimes observed for H51 and H22, but are somewhat more different, since the population of HNδ1 and HNε2 is most skewed for H31. In general, none of the three states of a histidine exists longer than about 20 μs. The lifetime of His^+ is the longest between pH 0 and pH 7.5 and the lifetimes of HNδ1 and HNε2 are the longest between pH 7 and 10. It should be noted that the longest lifetimes coincide with the biological relevant pH values around 7.4.

EXPERIMENTAL SECTION

Theory. The protonation processes of the histidine involve a coupled system of two titrating groups resulting in a macroscopic dissociation constant K_a with

$$K_a = [H^+]\frac{p_{HN\varepsilon 2} + p_{HN\delta 1}}{p_{His^+}} \quad (1)$$

and two microscopic, or site-specific, dissociation constants

$$K_{a,HN\varepsilon 2} = [H^+]\frac{p_{HN\varepsilon 2}}{p_{His^+}},\ K_{a,HN\delta 1} = [H^+]\frac{p_{HN\delta 1}}{p_{His^+}} \quad (2)$$

https://doi.org/10.1021/jacs.4c04647
J. Am. Chem. Soc. 2024, 146, 22284−22294

where p_i denotes the population of a given state, His$^+$, HNε2, or HNδ1.[40] The doubly deprotonated imidazolate was ignored because its pK_a value can be assumed to be higher than 14,[41] which was also confirmed for the *rhh* protein.[23] As a result, the population ratio of the neutral tautomers is constant:

$$\frac{p_{\mathrm{HN}\delta 1}}{p_{\mathrm{HN}\varepsilon 2}} = \frac{K_{\mathrm{a,HN}\delta 1}}{K_{\mathrm{a,HN}\varepsilon 2}} = K_{\mathrm{taut}} \tag{3}$$

The macroscopic dissociation constant K_a can be determined by analyzing the pH dependence of the chemical shifts via the Henderson−Hasselbalch equation. The site-specific dissociation constants can then be determined by substituting eqs 3 and 2 into (1):

$$K_{\mathrm{a,HN}\delta 1} = \frac{K_a}{1 + 1/K_{\mathrm{taut}}},\ K_{\mathrm{a,HN}\varepsilon 2} = \frac{K_a}{1 + K_{\mathrm{taut}}} \tag{4}$$

From these expressions it is evident that the site-specific dissociation constant must be less than or equal to K_a; consequently, the site-specific pK_a values are greater than the macroscopic pK_a.

Proton exchange with water can be described by the reaction scheme in Figure 6, in which His denotes the basic and His-H$^+$ the

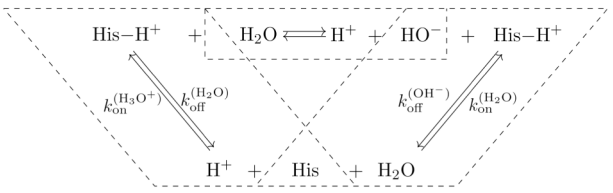

Figure 6. Reaction scheme for an acid−base equilibrium of histidine in water, modified with permission from ref 7. Copyright 1964 Wiley.

acid state of histidine. $k_{on}^{(H_3O+)}$ and $k_{off}^{(OH-)}$ are second order rate constants that include the H_3O^+ and OH^- concentration, respectively, while $k_{off}^{(H_2O)}$ and $k_{on}^{(H_2O)}$ appear as first order rate constants since the H_2O concentration can be seen as constant. The first and second order rate constants are related by

$$k_{off}^{(H_2O)} = k_{on}^{(H_3O+)} K_a \tag{5}$$

$$k_{on}^{(H_2O)} = k_{off}^{(OH-)} \frac{K_w}{K_a} \tag{6}$$

where K_w is the product of the hydronium and hydroxide concentrations.[7] For the pseudo two-state model and the H_3O^+/H_2O mediated exchange mechanism, the overall on- and off-rates are $k_{on} = k_{on}^{(H_3O+)}[H^+]$ and $k_{off} = k_{off}^{(H_2O)}$, while for the H_2O/OH^- mediated exchange they are $k_{on} = k_{on}^{(H_2O)}$ and $k_{off} = k_{off}^{(OH-)}[OH^-]$. The exchange rate is the sum of the on and off rate with $k_{ex} = k_{on} + k_{off}$. In cases where both pathways contribute simultaneously, k_{on} and k_{off} are simply the sums of the corresponding rates in each pathway.

The same formulas as above apply to each of the two protonation/deprotonation sites in a circular three state model.

Additionally, the ratios of the populations and rate constants are related as

$$\frac{p_{\mathrm{HN}\varepsilon 2}}{p_{\mathrm{His}^+}} = \frac{k_{\mathrm{off,HN}\varepsilon 2}}{k_{\mathrm{on,HN}\varepsilon 2}} \tag{7}$$

$$\frac{p_{\mathrm{HN}\delta 1}}{p_{\mathrm{His}^+}} = \frac{k_{\mathrm{off,HN}\delta 1}}{k_{\mathrm{on,HN}\delta 1}} \tag{8}$$

$$\frac{p_{\mathrm{HN}\delta 1}}{p_{\mathrm{HN}\varepsilon 2}} = \frac{k_{\mathrm{taut}\uparrow}}{k_{\mathrm{taut}\downarrow}} \tag{9}$$

where k_{on} and k_{off} are the overall on and off rates of the reaction steps connecting the protonated histidine and the corresponding tautomer, and $k_{taut\uparrow}$ is the rate of exchange between HNε1 to HNδ2, and vice versa for $k_{taut\downarrow}$.

$k_{taut\uparrow}$ was assumed to be either constant or dependent on the hydroxide concentration

$$k_{\mathrm{taut}\uparrow} = k_{\mathrm{taut}\uparrow}^{(H_2O)} + [OH^-] k_{\mathrm{taut}\uparrow}^{(OH-)} \tag{10}$$

For the pseudo two-state model (Ia or Ib), the measured transverse relaxation rate R_2 is given by[32]

$$R_2 = p_{\mathrm{His}^+} R_{2,\mathrm{His}^+} + p_{\mathrm{His}_{\mathrm{taut}}} R_{2,\mathrm{His}_{\mathrm{taut}}} + R_{\mathrm{ex}} \tag{11}$$

which depends on the intrinsic transverse relaxation rates of the individual states, R_{2,His^+} and $R_{2,His_{taut}}$, and the exchange rate, R_{ex}. $p_{His_{taut}}$ is the total population of the neutral states, and $R_{2,His_{taut}}$ is the averaged R_2 of the two tautomers, which in the pseudo two-state model are assumed to exchange rapidly.

In the fast exchange regime ($k_{ex} > \Delta\omega$), R_{ex} can be estimated by

$$R_{\mathrm{ex}} = \frac{p_{\mathrm{His}^+} p_{\mathrm{His}_{\mathrm{taut}}} \Delta\omega^2}{k_{\mathrm{ex}}} \left[1 - \frac{2\tanh(k_{\mathrm{ex}}\tau_{\mathrm{cp}}/2)}{k_{\mathrm{ex}}\tau_{\mathrm{cp}}}\right] \tag{12}$$

where $\Delta\omega$ is the frequency difference between the two populations and τ_{cp} the delay between refocusing pulses in the CPMG block.[26]

For the circular three-state model (IIIa+c, IIIb+c, IIIa+d, or IIIb +d), the relaxation was described by the Bloch-McConnell equation[42]

$$\frac{d\mathbf{M}^+(t)}{dt} = (i\boldsymbol{\Omega} - \mathbf{R} + \mathbf{K})\mathbf{M}^+(t) \tag{13}$$

K is a 3 × 3 exchange matrix with

$$\mathbf{K} = \begin{bmatrix} 0 & k_{\mathrm{on,HN}\varepsilon 2} & k_{\mathrm{taut}\uparrow} \\ k_{\mathrm{off,HN}\varepsilon 2} & 0 & k_{\mathrm{off,HN}\delta 1} \\ k_{\mathrm{taut}\downarrow} & k_{\mathrm{on,HN}\delta 1} & 0 \end{bmatrix} \tag{14}$$

and $\boldsymbol{\Omega}$ the diagonal matrix for the chemical shifts with $\Omega_{11} = \omega_{\mathrm{HN}\varepsilon 2}$, $\Omega_{22} = \omega_{\mathrm{His}^+}$, $\Omega_{33} = \omega_{\mathrm{HN}\delta 1}$. **R** the diagonal matrix for the intrinsic relaxation rates.

Protein Samples. The *rhh* protein from plasmid pRN1 of *Sulfolobus islandicus* was expressed in M9 minimal media and purified as described previously,[39] using 1.5 g/L ^{15}N NH_4Cl and 2 g/L $^{13}C_6$ glucose for standard double labeling and 2 g/L unlabeled glucose and 1 g/L 1-$^{13}C_1$ ribose for site-selective ^{13}C labeling of Hisδ2.[43] T4-Lysozyme was expressed in M9 minimal media and purified as described previously,[44] using2 g/L $^{13}C_6$ glucose. Samples were concentrated to 1 mM, the pH was adjusted with NaOH or HCl directly on each sample in water (10% D_2O) and checked right before and after the measurement in the NMR tube. pH values were measured at 22 °C using aninoLab pH 720 pH meter with a Hamilton Spintrode pH electrode.

NMR Spectroscopy. All ^{1}H and ^{13}C R_2 experiments were performed on a Bruker DRX 500 NMR spectrometer at a static magnetic field strength of 11.7 T and 23 °C, while ^{15}N R_2 experiments were recorded on a Bruker Avance III 600 NMR spectrometer at a magnetic field strength of 14.1 T and 25 °C. A CPMG refocusing frequency of 1000 Hz was applied in the R_2 experiments. Side chain ^{1}H R_2 experiments are based on aromatic ^{1}H CPMG relaxation dispersion experiments.[45] It has been established that ^3J ^{1}H−^{1}H couplings in His do not affect R_2.[45]. Side chain ^{13}C R_2 experiments are based on aromatic ^{13}C TROSY relaxation dispersion experiments.[46] Side chain ^{15}N R_2 experiments are measured by a HCN triple resonance[47] pulse sequence (Figure S5). It has been optimized with respect to longitudinal and transverse ^{13}C relaxation properties.[48] For H22, additional measurements were performed on a sample with site-selective His ^{13}Cδ2 labeling in 99% D_2O on a Bruker Avance III spectrometer at a static field of 18.8 T and 15 °C to slow down

https://doi.org/10.1021/jacs.4c04647
J. Am. Chem. Soc. 2024, 146, 22284−22294

exchange processes. All spectra were processed with NMRPipe[49] and analyzed with PINT.[50]

Data Analysis. Equilibrium properties of the histidines in the *rhh* protein[23] (pK_a values and populations of the HNδ1 and HNε2 tautomer for H22 and H51) and T4-Lysozyme[51] (pK_a value for H31) have been determined before and were confirmed in this study. For H22, the data reported by Raum et al.[23] were fitted together with the chemical shifts from ^{1}H CPMG relaxation dispersion experiments and the HCN triple resonance[47] pulse sequence (Figure S5) to improve the results for the dissociation constant and the chemical shift difference as already described.[23] These pH titration experiments allow the determination of the populations (His^+, HNδ1 and HNε2) at any pH value, as well as the chemical shift difference $\Delta\delta(H^+)$ (Table S1).

Furthermore, the individual populations of HNδ1 and His HNε2 can be estimated from $^{13}C\delta2$, $^{15}N\delta1$, and $^{15}N\varepsilon2$ and chemical shift differences for the tautomers from Platzer et al.[24] For H22, additional spectra were acquired in the slow exchange regime to directly measure the chemical shifts of each tautomer.

For the pseudo two-state model (Ia or Ib), data were fitted to eqs 11 and 12 with the H_3O^+/H_2O mediated exchange mechanism applied to H22 and H51 whereas the H_2O/OH^- mediated exchange model was applied to H31, based on eqs 5 and 6. Limits were imposed on $\Delta\omega$at ±2 SD from the reported random coil shift.[24] The pK_a of H51 was fitted without restrictions, whereas for H22 and H31 limits were set at ±1 SD of the chemical shift based pK_a, because of a shifted peak and missing baseline in the basic pH range, respectively.

For the circular three-state model (IIIa+c, IIIb+c, IIIa+d or IIIb +d), data were fitted numerically using eqs 13 and 14,with parameters from eqs 3−9, using in-house implementation in MATLAB described in ref[52]. To simplify the model, the diagonal elements of **R** were assumed equal.

For H22, k_{on} was assumed to be equal for the two tautomers based on their similar populations and similar R_2 vs pH profiles for $^{15}N\delta1$ and $^{15}N\varepsilon2$. For the unknown chemical shift differences between the neutral tautomers, a range from 50−200% of the values previously determined[24] were allowed for the ^{15}N positions and 75−150% for the $^{13}C\delta2$ position. At the end, the fitted values for the ^{15}N position were about 62−80% of the reference values and for the $^{13}C\delta2$ position about 106−113% of the reference value, except for H31 with 147% but with high uncertainty because of the small population of the HNε2 tautomer. Estimated and allowed population ranges for the HNε2 tautomer were 53−56%, 0−16% and 65−85% for H22, H31, and H51, respectively. For H22, it was based on measurements in the slow exchange range.

For error estimation, Monte Carlo simulations with 200 steps were executed for the three-state model and 1000 steps for the pseudo two-state model.

CONCLUSIONS

In this work we determined the intrinsic proton exchange kinetics of histidine side chains and the rate constants for interconversion among the three states (His^+, HNε2, and HNδ1). We find that proton transfer is very fast and reaches the diffusion limit. The dominant mechanism of proton exchange between histidine and the solvent switches from being proton mediated below pH 7.8 to hydroxide mediated at higher pH. There is direct proton exchange between the two neutral tautomeric forms, likely mediated by a bridging water molecule at low and neutral pH, or by hydroxide at high pH. We analyzed the resulting data together with previously reported exchange data on Asp and Glu to reveal free-energy relationships between thermodynamic and kinetic parameters (pK_a values and k_{on} or k_{off} rate constants) for the H_3O^+/H_2O mediated proton exchange mechanism. The results yield an estimate of the maximal exchange rates for a given pK_a value in the proton dominated pH range. For the histidine with a pK_a value of 7, our analysis enables the calculation of all its rate constants and lifetimes over the entire pH range. This provides a framework to investigate the mechanistic and catalytic potential of histidines in enzymatic acid/base catalysis.

ASSOCIATED CONTENT

Supporting Information

The Supporting Information is available free of charge at https://pubs.acs.org/doi/10.1021/jacs.4c04647.

Table of pK_a values and chemical shift differences determined from pH titration data, figures of exchange models, R_2 vs pH profiles for H31 with fits to model Ia, R_2 vs pH profiles for H51 with fits to model IIa, R_2 vs pH profiles for H51 with fits to model IIIa+d, NMR pulse sequence for the H(C)N L-TROSY ^{15}N R_2 experiment for imidazole (PDF)

AUTHOR INFORMATION

Corresponding Author

Ulrich Weininger − *Institute of Physics, Biophysics, Martin-Luther-University Halle-Wittenberg, Halle (Saale) D-06120, Germany*; orcid.org/0000-0003-0841-8332; Phone: +49 345 55 28555; Email: ulrich.weininger@physik.uni-halle.de; Fax: +49 345 55 27161

Authors

Heiner N. Raum − *Institute of Physics, Biophysics, Martin-Luther-University Halle-Wittenberg, Halle (Saale) D-06120, Germany*

Kristofer Modig − *Division of Biophysical Chemistry, Center for Molecular Protein Science, Department of Chemistry, Lund University, Lund SE-22100, Sweden*

Mikael Akke − *Division of Biophysical Chemistry, Center for Molecular Protein Science, Department of Chemistry, Lund University, Lund SE-22100, Sweden*; orcid.org/0000-0002-2395-825X

Complete contact information is available at: https://pubs.acs.org/10.1021/jacs.4c04647

Notes

The authors declare no competing financial interest.

ACKNOWLEDGMENTS

This research was supported by the Deutsche Forschungsgemeinschaft (WE 5587/1-1 & WE 5587/1-2) and the Swedish Research Council (2021-05591).

REFERENCES

(1) Reynolds, W. F.; Peat, I. R.; Freedman, M. H.; Lyerla, J. R. Determination of the tautomeric form of the imidazole ring of L-histidine in basic solution by carbon-13 magnetic resonance spectroscopy. *J. Am. Chem. Soc.* **1973**, *95* (2), 328−331.

(2) Li, S. H.; Hong, M. Protonation, Tautomerization, and Rotameric Structure of Histidine: A Comprehensive Study by Magic-Angle-Spinning Solid-State NMR. *J. Am. Chem. Soc.* **2011**, *133* (5), 1534−1544.

(3) Weininger, U.; Modig, K.; Geitner, A. J.; Schmidpeter, P. A. M.; Koch, J. R.; Akke, M. Dynamics of Aromatic Side Chains in the Active Site of FKBP12. *Biochemistry* **2017**, *56* (1), 334−343.

(4) Bartlett, G. J.; Porter, C. T.; Borkakoti, N.; Thornton, J. M. Analysis of catalytic residues in enzyme active sites. *J. Mol. Biol.* **2002**, *324* (1), 105−121.

(5) Holliday, G. L.; Mitchell, J. B. O.; Thornton, J. M. Understanding the Functional Roles of Amino Acid Residues in Enzyme Catalysis. *J. Mol. Biol.* **2009**, *390* (3), 560−577.
(6) Fersht, A. *Enzyme Structure and Mechanism*; W. H. Freeman, 1977.
(7) Eigen, M. Proton Transfer, Acid-Base Catalysis, and Enzymatic Hydrolysis. Part I: ELEMENTARY PROCESSES. *Angew. Chem., Int. Ed.* **1964**, *3* (1), 1−19.
(8) Buller, A. R.; Townsend, C. A. Intrinsic evolutionary constraints on protease structure, enzyme acylation, and the identity of the catalytic triad. *Proc. Natl. Acad. Sci. U. S. A.* **2013**, *110* (8), No. E653−E661.
(9) Rauwerdink, A.; Kazlauskas, R. J. How the Same Core Catalytic Machinery Catalyzes 17 Different Reactions: The Serine-Histidine-Aspartate Catalytic Triad of alpha/beta-Hydrolase Fold Enzymes. *ACS Catal.* **2015**, *5* (10), 6153−6176.
(10) Lindskog, S. Structure and mechanism of carbonic anhydrase. *Pharmacol. Ther.* **1997**, *74* (1), 1−20.
(11) Raum, H. N.; Fisher, S. Z.; Weininger, U. Energetics and dynamics of the proton shuttle of carbonic anhydrase II. *Cell. Mol. Life Sci.* **2023**, *80* (10), 286.
(12) Preimesberger, M. R.; Majumdar, A.; Rice, S. L.; Que, L.; Lecomte, J. T. Helix-Capping Histidines: Diversity of N-H···N Hydrogen Bond Strength Revealed by (2h)JNN Scalar Couplings. *Biochemistry* **2015**, *54* (46), 6896−6908.
(13) Krishna Deepak, R. N.; Sankararamakrishnan, R. N-H···N Hydrogen Bonds Involving Histidine Imidazole Nitrogen Atoms: A New Structural Role for Histidine Residues in Proteins. *Biochemistry* **2016**, *55* (27), 3774−3783.
(14) Jensen, M. R.; Hass, M. A.; Hansen, D. F.; Led, J. J. Investigating metal-binding in proteins by nuclear magnetic resonance. *Cell. Mol. Life Sci.* **2007**, *64* (9), 1085−1104.
(15) Styring, S.; Sjoholm, J.; Mamedov, F. Two tyrosines that changed the world: Interfacing the oxidizing power of photochemistry to water splitting in photosystem II. *Biochim. Biophys. Acta* **2012**, *1817* (1), 76−87.
(16) Pagba, C. V.; McCaslin, T. G.; Chi, S. H.; Perry, J. W.; Barry, B. A. Proton-Coupled Electron Transfer and a Tyrosine-Histidine Pair in a Photosystem II-Inspired beta-Hairpin Maquette: Kinetics on the Picosecond Time Scale. *J. Phys. Chem. B* **2016**, *120* (7), 1259−1272.
(17) Wang, J.; Tochio, N.; Kawasaki, R.; Tamari, Y.; Xu, N.; Uewaki, J.; Utsunomiya-Tate, N.; Tate, S. Allosteric Breakage of the Hydrogen Bond within the Dual-Histidine Motif in the Active Site of Human Pin1 PPlase. *Biochemistry* **2015**, *54* (33), 5242−5253.
(18) Hu, J.; Fu, R.; Nishimura, K.; Zhang, L.; Zhou, H. X.; Busath, D. D.; Vijayvergiya, V.; Cross, T. A. Histidines, heart of the hydrogen ion channel from influenza A virus: Toward an understanding of conductance and proton selectivity. *Proc. Natl. Acad. Sci. U. S. A.* **2006**, *103* (18), 6865−6870.
(19) Cohen, A.; Ben-Abu, Y.; Hen, S.; Zilberberg, N. A novel mechanism for human K2P2.1 channel gating. Facilitation of C-type gating by protonation of extracellular histidine residues. *J. Biol. Chem.* **2008**, *283* (28), 19448−19455.
(20) Pelton, J. G.; Torchia, D. A.; Meadow, N. D.; Roseman, S. Tautomeric States of the Active-Site Histidines of Phosphorylated and Unphosphorylated Iii(Glc), a Signal-Transducing Protein from Escherichia-Coli, Using 2-Dimensional Heteronuclear Nmr Techniques. *Protein Sci.* **1993**, *2* (4), 543−558.
(21) Vila, J. A.; Arnautova, Y. A.; Vorobjev, Y.; Scheraga, H. A. Assessing the fractions of tautomeric forms of the imidazole ring of histidine in proteins as a function of pH. *Proc. Natl. Acad. Sci. U. S. A.* **2011**, *108* (14), 5602−5607.
(22) Hass, M. A. S.; Mulder, F. A. A. Contemporary NMR Studies of Protein Electrostatics. *Annu. Rev. Biophys.* **2015**, *44*, 53−75.
(23) Raum, H. N.; Weininger, U. Experimental pK(a) Value Determination of All Ionizable Groups of a Hyperstable Protein. *ChemBiochem* **2019**, *20* (7), 922−930.
(24) Platzer, G.; Okon, M.; McIntosh, L. P. pH-dependent random coil H-1, C-13, and N-15 chemical shifts of the ionizable amino acids: A guide for protein pK (a) measurements. *J. Biomol. NMR* **2014**, *60* (2−3), 109−129.
(25) Palmer, A. G. NMR characterization of the dynamics of biomacromolecules. *Chem. Rev.* **2004**, *104* (8), 3623−3640.
(26) Palmer, A. G., 3rd; Kroenke, C. D.; Loria, J. P. Nuclear magnetic resonance methods for quantifying microsecond-to-millisecond motions in biological macromolecules. *Meth. Enzymol.* **2001**, *339*, 204−238.
(27) Korzhnev, D. M.; Religa, T. L.; Banachewicz, W.; Fersht, A. R.; Kay, L. E. A Transient and Low-Populated Protein-Folding Intermediate at Atomic Resolution. *Science* **2010**, *329* (5997), 1312−1316.
(28) Neudecker, P.; Robustelli, P.; Cavalli, A.; Walsh, P.; Lundstrom, P.; Zarrine-Afsar, A.; Sharpe, S.; Vendruscolo, M.; Kay, L. E. Structure of an Intermediate State in Protein Folding and Aggregation. *Science* **2012**, *336* (6079), 362−366.
(29) Weininger, U.; Modig, K.; Akke, M. Ring Flips Revisited: C-13 Relaxation Dispersion Measurements of Aromatic Side Chain Dynamics and Activation Barriers in Basic Pancreatic Trypsin Inhibitor. *Biochemistry* **2014**, *53* (28), 4519−4525.
(30) Dreydoppel, M.; Raum, H. N.; Weininger, U. Slow ring flips in aromatic cluster of GB1 studied by aromatic C-13 relaxation dispersion methods. *J. Biomol. NMR* **2020**, *74* (2−3), 183−191.
(31) Akke, M.; Weininger, U. NMR Studies of Aromatic Ring Flips to Probe Conformational Fluctuations in Proteins. *J. Phys. Chem. B* **2023**, *127* (3), 591−599.
(32) Wallerstein, J.; Weininger, U.; Khan, M. A.; Linse, S.; Akke, M. Site-Specific Protonation Kinetics of Acidic Side Chains in Proteins Determined by pH-Dependent Carboxyl (13)C NMR Relaxation. *J. Am. Chem. Soc.* **2015**, *137* (8), 3093−3101.
(33) Hass, M. A. S.; Hansen, D. F.; Christensen, H. E. M.; Led, J. J.; Kay, L. E. Characterization of conformational exchange of a histidine side chain: Protonation, rotamerization, and tautomerization of His61 in plastocyanin from Anabaena variabilis. *J. Am. Chem. Soc.* **2008**, *130* (26), 8460−8470.
(34) Farrjones, S.; Wong, W. Y. L.; Gutheil, W. G.; Bachovchin, W. W. Direct Observation of the Tautomeric Forms of Histidine in N-15 Nmr-Spectra at Low-Temperatures - Comments on Intramolecular Hydrogen-Bonding and on Tautomeric Equilibrium-Constants. *J. Am. Chem. Soc.* **1993**, *115* (15), 6813−6819.
(35) Alei, M.; Morgan, L. O.; Wageman, W. E.; Whaley, T. W. Ph-Dependence of N-15 Nmr Shifts and Coupling-Constants in Aqueous Imidazole and 1-Methylimidazole - Comments on Estimation of Tautomeric Equilibrium-Constants for Aqueous Histidine. *J. Am. Chem. Soc.* **1980**, *102* (9), 2881−2887.
(36) Hansen, A. L.; Kay, L. E. Measurement of histidine pK a values and tautomer populations in invisible protein states. *Proc. Natl. Acad. Sci. U. S. A.* **2014**, *111* (17), E1705−E1712.
(37) Sehgal, A. A.; Duma, L.; Bodenhausen, G.; Pelupessy, P. Fast Proton Exchange in Histidine: Measurement of Rate Constants through Indirect Detection by NMR Spectroscopy. *Chem.-Eur. J.* **2014**, *20* (21), 6332−6338.
(38) Marx, D. Proton transfer 200 years after von Grotthuss: Insights from ab initio simulations. *ChemPhyschem* **2006**, *7* (9), 1848−1870.
(39) Weininger, U.; Zeeb, M.; Neumann, P.; Low, C.; Stubbs, M. T.; Lipps, G.; Balbach, J. Structure-Based Stability Analysis of an Extremely Stable Dimeric DNA Binding Protein from Sulfolobus islandicus. *Biochemistry* **2009**, *48* (42), 10030−10037.
(40) McIntosh, L. P.; Naito, D.; Baturin, S. J.; Okon, M.; Joshi, M. D.; Nielsen, J. E. Dissecting electrostatic interactions in Bacillus circulans xylanase through NMR-monitored pH titrations. *J. Biomol. NMR* **2011**, *51* (1−2), 5−19.
(41) Yagil, G. The proton dissociation constant of pyrrole, indole and related compounds. *Tetrahedron* **1967**, *23* (6), 2855−2861.
(42) McConnell, H. M. Spin Density Matrices for Paramagnetic Molecules. *J. Chem. Phys.* **1958**, *28* (6), 1188−1192.
(43) Weininger, U. Site-selective C-13 labeling of histidine and tryptophan using ribose. *J. Biomol. NMR* **2017**, *69* (1), 23−30.

https://doi.org/10.1021/jacs.4c04647
J. Am. Chem. Soc. 2024, 146, 22284−22294

(44) Perry, L. J.; Wetzel, R. Unpaired Cysteine-54 Interferes with the Ability of an Engineered Disulfide to Stabilize T4-Lysozyme. *Biochemistry* **1986**, *25* (3), 733−739.
(45) Raum, H. N.; Dreydoppel, M.; Weininger, U. Conformational exchange of aromatic side chains by (1)H CPMG relaxation dispersion. *J. Biomol. NMR* **2018**, *72* (1−2), 105−114.
(46) Weininger, U.; Respondek, M.; Akke, M. Conformational exchange of aromatic side chains characterized by L-optimized TROSY-selected C-13 CPMG relaxation dispersion. *J. Biomol. NMR* **2012**, *54* (1), 9−14.
(47) Sudmeier, J. L.; Ash, E. L.; Gunther, U. L.; Luo, X. L.; Bullock, P. A.; Bachovchin, W. W. HCN, a triple-resonance NMR technique for selective observation of histidine and tryptophan side chains in C-13/N-15-labeled proteins. *J. Magn. Reson. B* **1996**, *113* (3), 236−247.
(48) Weininger, U.; Diehl, C.; Akke, M. C-13 relaxation experiments for aromatic side chains employing longitudinal- and transverse-relaxation optimized NMR spectroscopy. *J. Biomol. NMR* **2012**, *53* (3), 181−190.
(49) Delaglio, F.; Grzesiek, S.; Vuister, G. W.; Zhu, G.; Pfeifer, J.; Bax, A. NMRPipe: A multidimensional spectral processing system based on UNIX pipes. *J. Biomol. NMR* **1995**, *6* (3), 277−293.
(50) Ahlner, A.; Carlsson, M.; Jonsson, B. H.; Lundström, P. PINT: A software for integration of peak volumes and extraction of relaxation rates. *J. Biomol. NMR* **2013**, *56* (3), 191−202.
(51) Anderson, D. E.; Becktel, W. J.; Dahlquist, F. W. Ph-Induced Denaturation of Proteins - a Single Salt Bridge Contributes 3−5 kcal Mol to the Free-Energy of Folding of T4-Lysozyme. *Biochemistry* **1990**, *29* (9), 2403−2408.
(52) Weininger, U.; Modig, K.; Ishida, H.; Vogel, H. J.; Akke, M. Rotamer Jumps,Proton Exchange, and Amine Inversion Dynamics of Dimethylated Lysine Residues in Proteins Resolved by pH-Dependent (1)H and (13)C NMR Relaxation Dispersion. *J. Phys. Chem. B* **2019**, *123* (46), 9742−9750.

https://doi.org/10.1021/jacs.4c04647
J. Am. Chem. Soc. 2024, 146, 22284−22294